may have been from the west, as a current flowing eastward around the Cape of Good Hope (*18*), or through the "surfacing" of STW from below as the Agulhas Current weakened (*19*) or changed its course (*20*).

Why do these interpretations differ from those presented by Bé and Duplessy (*9*)? Analysis of the distribution of modern assemblages (*7, 8*) indicates that the transition between the subtropical and subpolar faunas coincides with the approximate location of the STC (Table 1), with the subpolar assemblage dominant south of the STC. Thus, if Bé and Duplessy's interpretations were correct, the subpolar assemblage should dominate the lower section of the core. Figure 2 shows that this fauna is never dominant. According to these criteria, the STC must have always been south of the core site. Furthermore, according to the criteria listed in Table 1, environmental estimates from both this report and (*9*) indicate the presence of STW, not SAW, during the coldest intervals. The criteria on which Bé and Duplessy's interpretations are based (*Orbulina universa* diameters) may not be as precisely defined as the criteria used in this report (*21*).

Tropical species dominate the fauna in the southwest Indian Ocean today and are associated with the continuous southward flow of the warm, low-salinity water along the African coast. Although tropical species were present during the last glacial maximum, the fauna was dominated by a subtropical assemblage. These faunal changes indicate that advection of tropical water into the region may have been less intense or more variable, or both, during glacial intervals than today. Comparison of these glacial assemblages with modern samples indicates that the region off the west coast of Australia may be a modern analog for the Agulhas region during glacial intervals. On the basis of this analogy, and estimated temperatures and salinities, I conclude that circulation in the Agulhas region during the last glacial period varied seasonally. A warm, southward-flowing current, similar to the Agulhas Current today but characterized by higher salinity, may have flowed southward during the summer months. During the winter months, however, this southward flow either decreased, shifted, or was replaced by a cool, high-salinity current from the south. This increased seasonal variability in current flow does not necessarily indicate an expansion or intensification of monsoon circulation throughout the Indian Ocean. In fact, computer simulations of ice-age climate (*22*) suggest that the southwest monsoon may have been weaker in the northern Indian Ocean. Instead, seasonal weakening or reversal of winds may have occurred within the region and may have affected surface circulation (*23*).

WILLIAM H. HUTSON

School of Oceanography, Oregon State University, Corvallis 97331

References and Notes

1. C. Duncan, thesis, University of Hawaii (1970).
2. M. Darbyshire, *Deep-Sea Res.* **13**, 57 (1966).
3. _____, *ibid.* **10**, 623 (1963).
4. G. E. R. Deacon, *Discovery Rep.* **15**, 1 (1937).
5. W. Hutson, *Mar. Micropaleontol.* **2**, 47 (1977); *Quat. Res. (N.Y.)* **9**, 87 (1978).
6. A. Bé and W. Hutson, *Micropaleontology* **23**, 369 (1977).
7. W. Hutson and W. Prell, *J. Paleontol.*, in press.
8. W. Prell, W. Hutson, D. Williams, *Mar. Micropaleontol.* **4**, 225 (1979).
9. A. W. H. Bé and J.-C. Duplessy, *Science* **194**, 419 (1976).
10. In the present study the cosine of the vector angle between modern and downcore samples is used as a similarity index [J. Imbrie and E. Purdy, *Mem. Am. Assoc. Pet. Geol. 1* (1962), p. 253]. This metric may be calculated by first normalizing each sample to unit length (that is, setting the sums of the squares equal to unity) and then calculating the cross product.
11. The environmental estimate, E, for a downcore sample is given by

$$\hat{E} = \frac{\sum_{i=1}^{ns} s_i \cdot e_i}{\sum_{i=1}^{ns} s_i}$$

where s_i is the faunal similarity between the downcore sample and the core-top sample i, e_i is the environmental value for sample i, and ns is the number of analogous modern samples used in the estimation. Tests based on the use of a modern set of core-top samples from the Indian Ocean (*7*) give the following standard errors for 152 estimates, based on the ten most similar analogs for each sample (that is, $ns = 10$): August sea-surface temperature, ± 1.34°C; February sea-surface temperature, ± 1.17°C; August sea-surface salinity, ± 0.47 per mil; and February sea-surface salinity, ± 0.42 per mil.
12. In tests carried out with the modern set of 152 core-top samples, confidence intervals were of the same order of magnitude as the residuals and positively correlated to the absolute value of the residuals ($P < .001$).
13. In addition, numerical experiments parallel to those outlined by W. Hutson [*Quat. Res. (N.Y.)* **8**, 355 (1977)] indicate that, if there are no modern analogs for a downcore sample, low-similarity indices or large confidence intervals, or both, would indicate that the resulting estimate may be erroneous.
14. J. Imbrie and N. Kipp, in *The Late Cenozoic Glacial Ages*, K. Turekian, Ed. (Yale Univ. Press, New Haven, 1971), p. 71. See also (*5, 7*).
15. Numerical comparisons, however, indicate that both techniques yield virtually identical estimates ($P < .001$).
16. D. J. Rockford, *Aust. J. Mar. Freshwater Res.* **20**, 1 (1969); B. V. Hamon, *Technical Paper No. 32* (Division of Fisheries and Oceanography, Commonwealth Scientific and Industrial Research Organization, Canberra, 1972), p. 1.
17. High-salinity estimates for glacial intervals may also reflect the effect of large continental ice sheets on global salinity.
18. Faunal data from a core (RC 11-86) off Cape Town, South Africa, indicates that subtropical conditions may have existed in the region during the last glacial maximum.
19. Darbyshire (*2*) reported that Agulhas waters often overlie subtropical waters, which may "surface" when flow in the Agulhas Current weakens.
20. On the basis of theoretical studies, G. Veronis [*J. Mar. Res.* **31**, 228 (1973)] suggests that increased wind stress could cause a western boundary current such as the Agulhas Current to become "detached" from the coast.
21. Examination of the data on which Bé and Duplessy based their interpretations [figure 2 of (*9*)] shows that the STC lies within a region where the average diameters are between 400 and 450 μm. At no time are the diameters less than 400 μm.
22. J. Williams, R. G. Barry, W. M. Washington, *J. Appl. Meteorol.* **13**, 305 (1974); W. Gates, *J. Atmos. Sci.* **33**, 1844 (1976); S. Manabe and D. Hahn, *J. Geophys. Res.* **82**, 3889 (1977).
23. For example, the ice-age simulation by Manabe and Hahn (*22*) indicates a change in both the direction and the intensity of the winds in the southwest Indian Ocean during the austral winter. These changes in the wind regime may have altered the wind stress over the Agulhas Current enough to cause the current to separate from the coast, as theorized by Veronis (*20*).
24. I thank A. Bé and his staff for their generous contribution of faunal data from core RC 17-69; I thank A. Bé, J.-C. Duplessy, W. Prell, and D. Williams for their useful comments and suggestions. I am grateful to D. McEwan for computational assistance, P. Lawrence for drafting, and G. Davis for typing services. This research was supported by NSF (International Decade of Oceanographic Exploration) grants DES 76-02202 and OCE 77-23162.

21 March 1979; revised 29 May 1979

Dislocations in Spinel and Garnet High-Pressure Polymorphs of Olivine and Pyroxene: Implications for Mantle Rheology

Abstract. *The meteorite Tenham was observed by transmission electron microscopy and ringwoodite and majorite, the high-pressure polymorphs of olivine and pyroxene, were identified. Ringwoodite contains antiphase boundaries and straight dislocations that are probably dissociated. Mantle flow of spinel might proceed by pure climb, and whole-mantle convection may be possible if the grain size is small enough.*

High-pressure syntheses have confirmed that olivine and pyroxene transform, respectively, to spinel and garnet structures (*1*). This transformation is compatible with seismic data and is thought to account for the 400-km discontinuity in the earth's mantle (*2*). Inasmuch as dislocations and stacking faults control the plastic flow properties of crystals (*3*), we began an investigation of the nature and structure of these defects in ringwoodite and majorite. Our purpose was to obtain a qualitative description of the rheology of high-pressure silicate phases and assess the possibility of deep-mantle convection.

We report here transmission electron microscopic observations of dislocations and extended defects in ringwoodite and majorite crystals. Ringwoodite is the high-pressure γ spinel polymorph of olivine, and majorite is the high-pressure

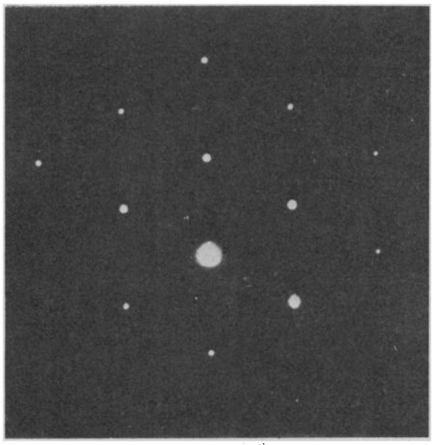

Fig. 1. Electron diffraction diagram of ringwoodite, (111) plane.

garnet polymorph of pyroxene. These minerals, which are metastable at ambient pressure, have been identified by x-ray diffraction in the shocked L6 chondritic meteorites Tenham (*4*), Catherwood (*5*), and Coorara (*6*). Ringwoodite and majorite grains in meteorites are the only available natural samples of the minerals, which probably constitute an important part of the mantle transition zone.

Petrographic thin sections were cut from a slice of the Tenham meteorite donated by the British Museum; purple grains of ringwoodite were optically identified in dark glassy veins, thinned by use of an ion beam, and examined in transmission at 100 kV in a EM 300 Philips electron microscope. We confirmed the crystal structure of the phases by electron diffraction (Fig. 1). Ringwoodite is indeed the γ spinel polymorph of olivine (*7*) and majorite is the garnet polymorph of pyroxene. The values determined for the cell parameters, a = 0.82 ± 0.02 nm for ringwoodite and a = 1.17 ± 0.02 nm for majorite, agree with the values determined by x-ray diffaction (*8*). In all the areas that we have examined ringwoodite grains are very small, ranging in size from 0.1 to 2 μm; their shape is often polygonal with grain boundaries parallel to {110} planes; and they coexist with majorite, which is present in greater amounts (*9*).

Fig. 2. Planar defects in a ringwoodite grain; scale bar, 0.2 μm.

The most conspicuous features in ringwoodite are extended planar defects that give rise to a fringed contrast when viewed obliquely (Fig. 2) (*10*). In grains with a {111} plane perpendicular to the electron beam, three families of these defects exist, intersecting the plane of the foil along ⟨112⟩ directions. The defects lie on {110} planes; contrast analysis shows that, for a defect lying on the (110) plane, the displacement vector is of the type $a/4$ $[1\bar{1}2]$, or equivalently $a/4$ [110] (*10*). These planar defects are therefore stacking faults, which can be considered either as Shockley-type faults corresponding to an $a/4$ $[1\bar{1}2]$ shear or as Frank-type faults corresponding to the removal of one neutral Mg_2SiO_4 layer with an accompanying $a/4$ [110] displacement (Fig. 3). This fault affects only the cationic sublattice and leaves the close-packed oxygen sublattice undisturbed; it can also be viewed as a twin boundary or as an antiphase boundary between domains where the cation order is reversed. It has been shown that this type of fault is the least energetic in the spinel structure (*11*), and indeed it has often been observed in other spinels such as $MgAl_2O_4$ (*12*), $LiFe_5O_8$ (*13*), and recently Mg_2GeO_4 (*14*, *15*). We think that the defects observed in ringwoodite may be considered as antiphase boundaries produced as the result of impingement of spinel domains nucleated at various places within one olivine crystal.

Dislocations in ringwoodite are best seen when the planar defects are out of contrast. The dislocation density is very nonuniform, varying from 10^9 dislocations per square centimeter in some grains to zero in others. So far, we have mostly observed straight dislocations lying along the three ⟨110⟩ directions in {111} planes (Fig. 4). In cases where their determination was possible, we found the Burgers vector to be $a/2$ $[0\bar{1}1]$ for dislocations lying along $[\bar{1}10]$ (the dislocation lines make a 60° angle with their Burgers vector). This is good evidence for the activity of $(111)[1\bar{1}0]$ slip systems. Similar observations have been made in $MgAl_2O_4$ spinel (*16*), where

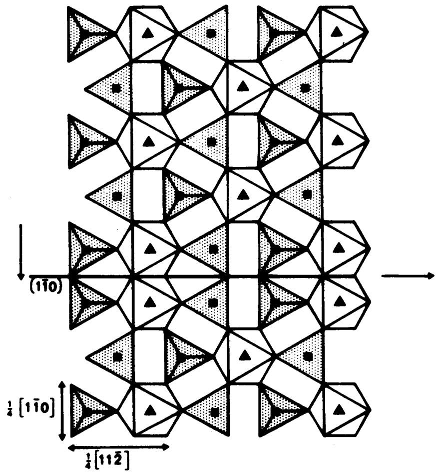

Fig. 3. Mixed layer (111) in the γ spinel structure. Silicon and magnesium ions are shown in tetrahedra and octahedra. Note their symmetrical disposition on each side of the $(1\bar{1}0)$ fault plane, seen edge-on horizontally. The $[11\bar{2}]$ direction is horizontal, the $[1\bar{1}0]$ direction vertical.

$(110)[1\bar{1}0]$ or $(111)[1\bar{1}0]$ slip systems have been found depending on the orientation of the crystal with respect to the applied stress. For the $(111)[1\bar{1}0]$ slip systems, a weak-beam analysis (*17*) showed that the 60° dislocations were dissociated according to the reaction $a/2$ $[1\bar{1}0] \rightarrow a/4$ $[1\bar{1}0] + a/4$ $[1\bar{1}0]$, with a fault of the type (001) $a/4$ $[0\bar{1}1]$ on the (001) plane, which is the least energetic fault (*11*).

Majorite shows very little defect structure; indeed, most of the crystals are dislocation-free. When dislocations are seen, their density is very low, in keeping with the fact that garnet is very resistant to deformation. The dislocations observed, in majorite as well as in ring-

Fig. 4. Straight dislocations along $[1\bar{1}0]$ in the (111) plane of ringwoodite; scale bar, 0.1 μm.

woodite, are typical of crystals annealed at high temperatures, whereas neighboring untransformed olivine has a high density of dislocations corresponding to the (110)[001] slip system typical of shocked crystals (*17*); this is to be expected since the high-pressure phases grew in replacement of shocked minerals. The positive identification of ringwoodite and majorite in a shocked meteorite supports the view that it is possible to synthesize high-pressure silicate phases by shock wave experiments.

Although our observations on ringwoodite are still fragmentary, they all point to a remarkable similarity to other spinels; we find the same stacking faults and the same slip systems as in $MgAl_2O_4$ spinel, for instance. It seems reasonable to think that many other similarities will eventually be found; thus we expect to find straight edge dislocations with an $a/4$ [110] Burgers vector, dissociated in their climb plane (110) with the least energetic fault (*16, 18*). If this is the case, we may venture to draw a few tentative conclusions regarding the rheology of the mantle transition zone (*19*): intracrystalline flow of γ spinel may proceed by slip on (111) planes (probably difficult and controlled by pinching of the stacking fault which does not lie in the glide plane) or by pure climb of edge dislocations dissociated in their climb planes (*17, 18*). If the grain size of spinel is small in the mantle (*19*), it is possible to consider grain-boundary sliding accommodated by Nabarro or Coble creep in the grains as an important flow mechanism (*20*); this would make it possible to think that the mantle viscosity does not increase much in the transition zone (*21*) and that there is no rheological barrier to convection below 400 km (*22*).

MICHEL MADON, JEAN-PAUL POIRIER
Institut de Physique du Globe,
Université Paris VI,
75230 Paris Cedex 05, France

References and Notes

1. A. E. Ringwood and A. Major, *Phys. Earth Planet. Inter.* **3**, 89 (1970).
2. D. L. Anderson, *Annu. Rev. Earth Planet. Sci.* **5**, 179 (1977).
3. A. Nicolas and J. P. Poirier, *Crystalline Plasticity and Solid State Flow in Metamorphic Rocks* (Wiley-Interscience, New York, 1976).
4. R. A. Binns, R. J. Davis, S. J. B. Reed, *Nature (London)* **221**, 943 (1969); R. A. Binns, *Phys. Earth Planet. Inter.* **3**, 156 (1970).
5. L. C. Coleman, *Can. Mineral.* **15**, 97 (1977).
6. J. V. Smith and B. Mason, *Science* **168**, 832 (1970).
7. J. P. Poirier and M. Madon, *Eos* **60**, 370 (1979).
8. The cell parameters determined in this work seem a little larger than those determined by x-ray diffraction (*1*); this is certainly due to the fact that selected-area electron diffraction is less accurate than x-ray diffraction. Electron diffraction, however, has the great advantage of giving direct, unambiguous information on the reciprocal lattice.
9. R. Jeanloz [*Proc. 10th Lunar Planet. Sci. Conf.* (1979), p. 619] reported that he could find no spectroscopic evidence for ringwoodite in the purple grains of Catherwood, whereas majorite could be identified. He tentatively attributes this to the fact that ringwoodite is intimately mixed with abundant majorite (R. Jeanloz, personal communication).
10. Contrast analysis uses the fact that the contrast of the defect vanishes when its displacement vector is normal to the reciprocal lattice vector used to produce the image. Thus for most imaging conditions only two out of three families of defects are simultaneously visible.
11. P. Veyssière, J. Rabier, J. Grilhé, *Phys. Status Solidi A* **31**, 605 (1975).
12. M. H. Lewis, *Philos. Mag.* **14**, 1003 (1966). In this case the defects were parallel to {100} planes.
13. O. van der Biest and G. Thomas, *Phys. Status Solidi A* **24**, 65 (1974).
14. P. J. Vaughan and D. L. Kohlstedt, *Eos* **60**, 370 (1979).
15. In Mg_2GeO_4 and $LiFe_5O_8$ the defects on {110} planes appear in exactly the same zigzag pattern as in Fig. 2. In ringwoodite, we were always able to give a consistent analysis of the triple junctions by using the fault vector determined by contrast analysis.
16. N. Doukhan, R. Duclos, B. Escaig, *J. Phys.* **40**, 381 (1979).
17. J. R. Ashworth and D. J. Barber, *Philos. Trans. R. Soc. London Ser. A* **286**, 493 (1977).
18. P. Veyssière, J. Rabier, H. Garem, J. Grilhé, *Philos. Mag. A* **38**, 61 (1978). Climb splitting of edge dislocations has also been observed in magnesium [J. F. Stohr and J. P. Poirier, *ibid.* **25**, 1313 (1970)].
19. It must be kept in mind that olivine and ringwoodite in Tenham have the composition $(Mg_{0.76}Fe_{0.24})_2SiO_4$. The iron content is therefore higher than in the mantle, probably too high for β spinel to exist. Our conclusions should be restricted to the upper part of the transition zone (below 400 km, before the iron-rich γ spinel that is first formed transforms to β spinel by a peritectic reaction) or to its lower part, when the β phase is transformed back to γ spinel. In both cases the spinel grain size may be quite small because nucleation may be more active than growth and because the grain size must be stabilized by other phases.
20. This is the so-called superplastic creep. P. J. Vaughan [*Eos* **59**, 1185 (1978); personal communication] experimentally found that Mg_2GeO_4 spinel deformed by this mechanism.
21. R. J. O'Connell [*Tectonophysics* **38**, 119 (1977)] pointed out such a possibility for the postspinel lower mantle.
22. G. F. Davies, *Geophys. J. R. Astron. Soc.* **49**, 459 (1977).
23. We thank R. Hutchison (British Museum) for providing the sample; A. Nicolas for having the thin sections prepared; C. Guillemin for help with the transmission electron microscopy; C. Willaime, M. Gandais, and N. Doukhan for useful discussions; and C. J. Allègre for reviewing the manuscript. This work was supported by Action Thématique Programmeé Géodynamique 1979. This is Institut de Physique du Globe contribution NS 336.

5 July 1979; revised 27 August 1979

Mouse Leukemia: Therapy with Monoclonal Antibodies Against a Thymus Differentiation Antigen

Abstract. *Monoclonal antibodies against a thymus cell differentiation antigen (Thy-1.1) were effective in the therapy of a transplanted mouse leukemia. Passive immunization resulted in high titers of cytotoxic antibody in the serum of treated mice and the suppression of metastatic tumor cells. The tumor-suppressive effects of the monoclonal antibodies were amplified by the administration of exogenous complement. This combined antibody and complement therapy resulted in the cure of leukemia in a significant proportion of the treated animals.*

The treatment of malignant disease with antibody has been of considerable interest to oncologists and immunologists throughout the past decade (*1*). Although inhibition of tumor growth has been demonstrated in experimental systems by the passive administration of antibody, these effects were usually found to be minimal, short-lived, or therapeutic against only small tumors. Solid tumors were relatively resistant to antibody therapy, whereas tumors of lymphoid origin were found more responsive. One of the limiting factors in the success of antibody therapy has been the lack of sufficiently high-titered antibodies of defined class, avidity, and specificity. In fact, the overall difficulties associated with these technical aspects have tended to dampen the enthusiasm for a more generalized approach to the serotherapy of cancer.

A reappraisal of the role of serotherapy in the treatment of tumors may now be warranted. With recent advances in somatic cell hybridization techniques (*2*) it is now possible to obtain permanent cell lines that continuously produce monoclonal antibodies of defined specificity. This is accomplished by the hybridization of B lymphocytes from immunized donors with myeloma cells in culture (*2*). Antibodies obtained from these hybrid cell lines are chemically homogeneous, react with constant avidity to single antigenic determinants, and can be isolated in quantities previously not obtainable by conventional methods. In this study we demonstrate that monoclonal antibodies directed against a T cell differentiation antigen (Thy-1.1) dramatically inhibit the growth of a transplantable AKR mouse lymphoma.

Mice of the AKR, 129, and C57BL/6 (B6) strains were purchased from the Jackson Laboratory. F_1 hybrids [(129 × AKR)F_1 and (B6 × AKR)F_1] prepared between these strains were bred in our mouse colony. The AKR SL2 leukemia (used for serotherapy) was derived from a spontaneous thymoma (*3*); SL2 cells passaged both in vivo and in vitro expressed high concentrations of Thy-1.1 antigen on the cell surfaces.

Hybrid cells producing monoclonal antibodies against the Thy-1.1 antigen were isolated from a fusion performed with BALB/c MOPC21 NSI/1 myeloma

